

## EXPERIMENTS AND NUMERICAL SIMULATIONS FOR LAMINAR, TRANSITIONAL AND TURBULENT FLOW OVER A BACKWARD-FACING STEP

### **Bruno A. Gomes**

Dept. Mech. Eng., PUC-Rio, bgomes@mec.puc-rio.br

### **Juliana K. Abrantes**

Dept. Mech. Eng., PUC-Rio, juliana@mec.puc-rio.br

### **Pedro C. Rabello**

Dept. Mech. Eng., PUC-Rio, rabello@mec.puc-rio.br

### **Arturo Jesus Ortega Malca**

Dept. Mech. Eng., PUC-Rio, tupamaru@mec.puc-rio.br

### **Angela Ourivio Nieckele**

Dept. Mech. Eng., PUC-Rio, nieckele@mec.puc-rio.br

### **Luis Fernando A. Azevedo**

Department of Mechanical Engineering, Pontifical Catholic University of Rio de Janeiro, 22453-900 – Rio de Janeiro, RJ, Brazil  
lfaa@mec.puc-rio.br

**Abstract.** *The two-dimensional flow field of water over a backward-facing step was investigated experimentally using particle image velocimetry. The objective of the study was to map the details of the flow field for different Reynolds numbers in the laminar, transition and turbulent regimes. The range of Reynolds numbers investigated based on the channel hydraulic diameter was from, 1000 to 13800. The experimental results were obtained as part of a program to form a bank of experimental data for validating numerical codes for predicting turbulent flows. The results obtained encompassed time-averaged velocity profiles at different axial stations along the center plane of the backward-facing step channel, as well as, instantaneous whole field measurements. Numerical calculations using the  $k-\epsilon$  RNG turbulence model were obtained and compared with the time-averaged experimental results. The agreement between measured and predicted velocity field was excellent for the laminar regime. For transition regime the agreement was poor for the region within the zone of recirculating flow downstream of the backstep. Better predictions were obtained for the turbulent regime. Instantaneous experimental results revealed the high degree of unsteadiness of the flow for the transition regime in the zone of recirculating flow.*

**Keywords.** *Backward-facing step, Turbulence modeling, PIV measurements*

### **1. Introduction**

The phenomena of separation and reattachment in internal flows have important engineering implications, being also of relevance for fundamental studies in fluid mechanics. In the class of internal flows, the flow over a backward-facing step has received considerable attention in the literature, having turned into a benchmark problem for assessing the predicting capabilities of turbulence models (e.g., Armaly et al, 1983, Kaiktsis et al, 1996, Le et al, 1997 and Tylli et al, 2002).

Armaly et al, 1983, have conducted a detailed investigation of flow over backward-facing steps using laser-Doppler anemometry to produce information on time-averaged velocity profiles. The authors investigated the laminar, transitional and turbulent flow regimes and mapped the main zone of recirculating flow formed downstream of the step location. The size of these zones was shown to increase sharply with Reynolds number for the laminar regime ( $Re < 1200$ ), decreasing continuously in the transition regime ( $1200 < Re < 6200$ ) and increasing again slightly and stabilizing for the turbulent regime ( $Re > 6200$ ). The presence of additional zones of recirculating flow, one downstream of the main zone and other located on the wall opposite to the step, was also verified. In the same work, two-dimensional numerical simulations of the flow over a backward facing step are presented and compared to the experimental results. It is demonstrated that both results agree well only up to Reynolds number of the order of 400. Beyond that, the predicted velocity profiles deviate from the measured ones, the reason being attributed to three-dimensional effects present in the flow.

A direct numerical simulation of flow over a backward-facing step for  $Re = 5100$  was presented in Le et al, 1997. The expansion ratio investigated (ratio between dimensions of the larger and smaller channels) was 1.2, compared to 1.94 of the experiments described above. Also, the ratio between the spanwise dimension of the channel to the step height was small, what imposed a strong three-dimensional character to the flow. The results obtained demonstrated that the reattachment line oscillated and varied in the spanwise direction. The velocity profiles in the recovery region

were shown to fall below the universal log-law, indicating that the turbulent boundary layer was not fully recovered after 20 step heights downstream of the separation point.

Sidewall effects on flow over backward-facing steps have recently been studied by Tylli et al, 2002. This study investigated both numerically and experimentally flows in a channel with an expansion ratio of 2 and aspect ratio of 20. Despite the large aspect ratio of the channel, the results demonstrated that the presence of the sidewalls induce the formation of a wall-jet at the lower wall directed toward the channel center plane. The intensity of this secondary flow increases with Reynolds for the laminar regime and decreases with Reynolds for the transitional and turbulent regimes.

The present study reports the results of an ongoing research program on flow over backward-facing steps, aimed at producing a data bank of results for the validation of numerical codes. In particular, the objective is to provide instantaneous and time-averaged velocity data at the center plane of the channel for a range of Reynolds numbers encompassing the laminar, transitional and turbulent regimes. At this stage of the research, the experimental data are compared with two-dimensional, steady-state numerical solutions in order to assess the influence of spatial and temporal characteristics of the flow. To this end, the experiments were designed to make use of a Particle Image Velocimetry system for velocity measurements. This is the only technique capable of providing instantaneous velocity data over an extensive region of the flow, producing valuable information on the flow structure. In the present paper center plane velocity fields for steady-state conditions are compared to the time-averaged velocity experiments. The discrepancies between measured and predicted results are explained with the aid of the instantaneous experimental results obtained with the PIV technique. Following is a description of the experimental setup and numerical simulations employed.

## 2. Experiments

### 2.1 The test section

The experiments were conducted in the test section shown schematically in Fig 1. The test section was specially designed to allow the utilization of optical techniques such as Laser-Doppler Velocimetry and Particle Image Velocimetry for the determination of the velocity field. In the present paper, only PIV data will be reported. Water was the working fluid and was circulated in closed loop by means of a centrifugal pump. A calibrated rotameter was used to determine the flow rate.

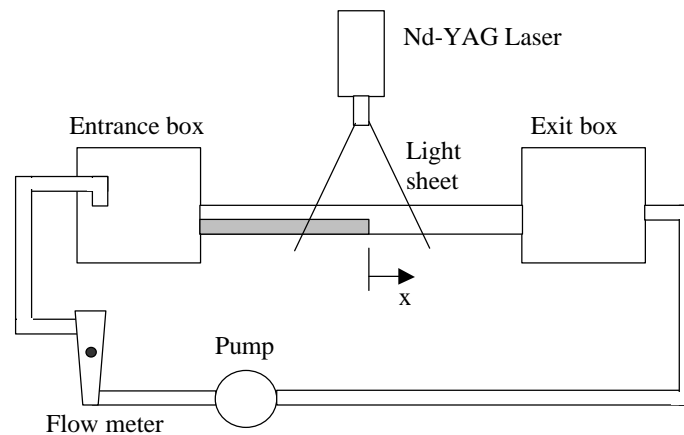


Figure 1. Schematic view of the test section.

The backward-facing step geometry was formed inside a long Plexiglas rectangular channel with dimensions of 30×300×2500 mm (height × width × length). The side walls of the channel were machined to within ± 0.1 mm so that the top and bottom walls of the channel could be considered parallel to each other, and the channel cross-sectional area could be considered uniform throughout the channel length. The channel was connected to two large Plexiglas boxes that provided space for accommodation of the inlet and outlet flows. Each box had dimensions of 400×400×400 mm. The boxes were connected to the centrifugal pump by means of 32-mm, PVC pipes. The pipes entered the inlet and outlet boxes through the wall opposite to the rectangular channel opening. In the case of the entrance box, a 90° curve was installed at exit section of the pipe. This curve directed the incoming flow away from the channel entrance, in order to avoid the formation of a jet-like flow in the channel entrance that could disturb the development process of the velocity profile. A 12-mm-thick and 1500-mm-long Plexiglas plate was inserted into the channel and affixed to one of the main walls of the channel. The width of the plate was equal to the width of the channel. The beginning of the plate was aligned with the inlet section of the channel, thereby reducing the through flow cross sectional area in the first part of the channel and forming the desired backstep geometry at the end of the plate. The final dimension of the backstep formed are:  $h = 18$  mm,  $H = 30$  mm,  $S = 12$  mm,  $L_1 = 1500$  mm,  $L_2 = 1000$  mm and  $L_3 = 300$  mm. These dimensions yield an expansion rate,  $H/h = 1.67$ , and an aspect ratio,  $L_3/h = 16.7$ .

In order to improve the quality of the optical access to the flow in the test section, part of the Plexiglas walls around the backstep region were machined and replaced by borosilicate glass plates. Special care was taken during the machining of the plexiglass walls and the installation of the glass windows so that no steps were formed at the junction of the glass windows and Plexiglas walls. For the PIV measurements (see next section) optical accesses through two adjacent orthogonal walls are needed. In the present case the laser light sheet passed through the glass window installed in the lateral wall, while the camera imaged the flow through the glass window installed in one of the side walls.

## 2.2 Velocity measurements

Instantaneous and time-averaged velocity and vorticity fields were obtained in the experiments. A Particle Image Velocimetry system was employed to obtain the desired flow characteristics. In this technique an extensive region of the flow is illuminated by a pulsed sheet of laser light of elevated intensity, revealing the image of small tracer particles previously distributed in the fluid. A digital camera mounted orthogonally to the light sheet records the position of the tracer particles at two close instants. A synchronization circuit coordinates the laser pulse with the camera capture, so that the two images are registered in consecutive frames. The particle displacements are determined by analyzing small sub-regions of the image (interrogation spots) and cross-correlating the image intensity distribution in the two frames. This process yields the mean particle displacement for each interrogation spot. The instantaneous velocity field is obtained by dividing the instantaneous displacement field by the time interval between laser pulses and by the magnification factor of the optical setup utilized.

In the present experiments a PIV system manufactured by TSI Inc, was utilized. This system employed a pair of integrated New Wave, frequency-doubled, Nd-YAG lasers capable of delivering up to 120 mJ of energy per pulse, at 15 Hz. The light sheet employed was formed by a cylindrical lens of  $-25$  mm focal distance to form the light plane, followed by a spherical lens of 500 mm focal distance to decrease the sheet thickness. Measurements were made at the light sheet waist with an approximate thickness of 0,3 mm. In order to maintain the accuracy of the velocity measurements, the camera was positioned at a distance from the light sheet that produced a magnification of approximately 1/6. Because of that, the extension of the flow captured in the streamwise direction was limited to approximately 60 mm. To allow the capture of the whole recirculation zone that follows the backstep, four displaced velocity fields were measured for each value of the Reynolds number investigated. This was achieved by sliding the camera in the streamwise direction. The matching of the four velocity fields was facilitated by imaging a scale attached to the exterior part of the test section. When this velocity field matching is used, only time averaged fields can be obtained. Typically, 30 instantaneous velocity fields were averaged in each of the four locations for each Reynolds number, and then the average fields were assembled together. Instantaneous information were computed for each individual axial location.

The camera employed was a TSI model 10-30 with resolution of 1000 x 1000 pixels using a 60-mm Nikor lens. Synchronization between the laser and the camera was controlled by a TSI model 60006 unit. The particle images were captured and processed by the Insight software manufactured by TSI Inc. Calibration studies conducted with a solid body rotation experiment (Gomes et al, 2000) revealed that an accuracy of the order of  $\pm 1\%$  is to be expected for the velocity measurements. Detailed information on the PIV technique can be found in several review publications (e.g., Raffel et al, 1998).

## 3. Mathematical Modeling

The computational domain, illustrated in Fig. 2, was defined with the same geometric parameters as the experimental setup. The channel length after the step was set as 30 S, where  $S = H - h$  is the step height. The length of the inlet channel in the calculations was taken as 1.17 S. The conservation equation were solved with the commercial software FLUENT. Only for Reynolds number equal to 1000, the flow was considered laminar, otherwise a turbulence model was activated. The turbulence model selected was the  $\kappa$ - $\epsilon$  RNG model for high Reynolds number, with a non-equilibrium wall law, sensitive to the pressure gradient.

The time average continuity and linear momentum conservation equation are

$$\frac{\partial \bar{u}_i}{\partial x_i} = 0 \quad \frac{\partial \mathbf{r} \bar{u}_j \bar{u}_i}{\partial x_j} = -\frac{\partial \bar{P}}{\partial x_i} + \frac{\partial}{\partial x_j} [m_{ef} (\frac{\partial \bar{u}_i}{\partial x_j} + \frac{\partial \bar{u}_j}{\partial x_i})] \quad (1)$$

where  $\bar{u}_i$  is the time average velocity component,  $\bar{P} = \bar{p} + (2/3) \mathbf{r} \mathbf{k}$  is a modified pressure, where  $\bar{p}$  is the pressure,  $\mathbf{k}$

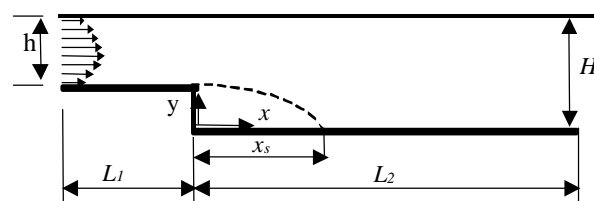


Figure 2. Test section and computational domain.

is the turbulent kinetic energy,  $\mathbf{m}_t = \mathbf{m} + \mathbf{m}$  is the effective turbulence viscosity,  $\mathbf{m}$  is the absolute and  $\mathbf{m}$  is the turbulent viscosity, given by

$$\mathbf{m}_t = \mathbf{r} C_m \mathbf{k}^2 / \mathbf{e} \quad (2)$$

The conservation equations of the turbulent kinetic energy  $\mathbf{k}$  and its dissipation ratio  $\mathbf{e}$  for the  $\kappa$ - $\epsilon$  RNG model are

$$\frac{\partial}{\partial x_j} (\mathbf{r} \mathbf{k} \bar{u}_j) = \frac{\partial}{\partial x_j} [\Gamma_{\mathbf{k}} \frac{\partial \mathbf{k}}{\partial x_j}] + G_{\mathbf{k}} - \mathbf{r} \mathbf{e} \quad \frac{\partial}{\partial x_j} (\mathbf{r} \mathbf{e} \bar{u}_j) = \frac{\partial}{\partial x_j} [\Gamma_{\mathbf{e}} \frac{\partial \mathbf{e}}{\partial x_j}] + C_{1e} \frac{\mathbf{e}}{\mathbf{k}} G_{\mathbf{k}} - C_{2e} \mathbf{r} \frac{\mathbf{e}^2}{\mathbf{k}} - R \quad (3)$$

$$G_{\mathbf{k}} = \mathbf{m} \left( \frac{\partial \bar{u}_i}{\partial x_j} + \frac{\partial \bar{u}_j}{\partial x_i} \right) \frac{\partial \bar{u}_i}{\partial x_j} \quad \Gamma_{\mathbf{k}} = \mathbf{m} + \mathbf{m}_t / \mathbf{s}_k \quad \Gamma_{\mathbf{e}} = \mathbf{m} + \mathbf{m}_t / \mathbf{s}_e \quad (4)$$

$$R = \mathbf{r} \frac{\mathbf{e}^2 C_m \mathbf{h}^3 (1 - \mathbf{h} / \mathbf{h}_o)}{\mathbf{k} (1 + \mathbf{b} \mathbf{h}^3)} \quad \mathbf{h} \equiv |S_{ij}| \mathbf{k} / \mathbf{e} \quad (5)$$

The empirical constants are:  $C_m = 0.0845$ ;  $C_{1e} = 1.42$ ;  $C_{2e} = 1.68$ ;  $\mathbf{s}_k = 1.393$ ;  $\mathbf{s}_e = 1.392$ ,  $\mathbf{h}_o = 4.38$ ;  $\mathbf{b} = 0.012$

The non-equilibrium wall function sensitized to pressure gradient is

$$\hat{u} = (1/k) \ln(E \hat{y}) \quad \hat{u} = (\tilde{u} / u_t)(u^* / u_t) \quad u_t = \sqrt{\mathbf{t}_w / \mathbf{r}} \quad (6)$$

$$\tilde{u} = u - \frac{1}{2} \frac{dp}{dx} \left[ \frac{y u}{\mathbf{r} k \sqrt{\mathbf{k}}} \ln \left( \frac{y}{y_u} \right) + \frac{y - y_u}{\mathbf{r} k \sqrt{\mathbf{k}}} + \frac{y u^2}{\mathbf{m}} \right] \quad \hat{y} = \mathbf{r} u^* y / \mathbf{m} \quad u^* = C_m^{1/4} \mathbf{k}^{1/2}$$

$$y_u = \hat{y} \mathbf{m} / (\mathbf{r} u^*)$$

where  $k = 0.42$  is the von Kármán constant,  $E = 9.793$  is an empirical constant,  $\mathbf{t}_w$  is the wall shear stress,  $u^*$  and  $u_t$  are friction velocities, and  $\tilde{u}$  and  $\hat{y}$  are dimensionless velocity and distance.

The kinetic energy equation at the wall-neighboring cells are solved assuming a two-layer concept, i.e., a viscous sublayer and a fully turbulent layer, defined as

$$\mathbf{t}_t = \begin{cases} 0, & y < y_u \\ \mathbf{t}_w, & y > y_u \end{cases} \quad \mathbf{k} = \begin{cases} (y / y_u)^2 \mathbf{k}_P, & y < y_u \\ \mathbf{k}_P, & y > y_u \end{cases} \quad \mathbf{e} = \begin{cases} (2u\mathbf{k}) / y^2, & y < y_u \\ \mathbf{k}^{3/2} / (C_\ell y), & y > y_u \end{cases} \quad (7)$$

where  $C_\ell = k C_m^{-3/4}$ . Using these profiles, the production of  $\mathbf{k}$  and  $\mathbf{e}$  at the near wall cell are determined by

$$G_{\mathbf{k}} = \frac{1}{y_n} \int_0^{y_n} \mathbf{t}_t \frac{\partial u}{\partial y} dy = \frac{\mathbf{r}}{k} \frac{u_t^4}{y_n u^*} \ln \left( \frac{y_n}{y_u} \right) \quad \mathbf{e}_P = \frac{1}{y_n} \int_0^{y_n} \mathbf{e} dy = \frac{\mathbf{k}_P}{y_n} \left[ \frac{2u}{y_u} + \frac{\mathbf{k}_P^{1/2}}{C_\ell} \ln \left( \frac{y_n}{y_u} \right) \right] \quad (8)$$

where  $y_n$  is the cell height ( $y_n = 2 y_p$ ).

The commercial software Fluent employed to solve the problem is based on the finite volume method (Patankar 1980). The "Power-law" interpolation scheme was selected, and the pressure-velocity coupling was handled by SIMPLE algorithm. A non-uniform mesh of  $200 \times 100$  was employed in the  $x$  and  $y$  directions, with the grids concentrated near the walls.

For the convergence of the numeric solution, the residues of the equations of mass conservation, momentum as well as the inherent equations to the turbulent models were controlled. The solution was considered converged when the residue went lower than  $10^{-10}$ .

#### 4. Results and Discussion

In this session the experimental and numerical results obtained will be presented. Time-averaged experimental results will be compared with the two-dimensional numerical solutions. Instantaneous results for the velocity field obtained from the PIV experiments will also be presented. The channel geometry was maintained fixed throughout the experiments with an expansion ratio  $H/h$  equal to 1.67. Six values of the Reynolds number based on the channel hydraulic diameter,  $2h$ , were investigated, namely,  $Re = 1000$ , in the laminar regime,  $Re = 3600$ , in the transition regime, and in the turbulent regime Reynolds numbers of 6200, 8800, 11400, and 13800.

Figure 3 was prepared to convey information on the experimental velocity profiles approaching the backstep location. Due to the long development length provided in the test section, it was expected that these profiles would be hydrodynamically fully developed just upstream of the step. These profiles were used as input to the numerical simulations conducted. In the figure, the axial velocity normalized by the maximum velocity is presented as a function of the non-dimensional cross stream coordinate  $y/S$ , where  $S$  is the step height. With this non-dimensional variable the lower wall of the smaller channel is located at  $y/S = 1$  while the upper wall is located at  $y/S = 2.5$ . In order not to overcrowd the figure, velocity profiles for only three different values of the Reynolds numbers are presented, namely, 1000, 3600, and 13800. These values were chosen to represent, respectively, the laminar, transition and turbulent regimes. For each value of the Reynolds number, two velocity profiles are presented for two different axial locations:  $x/S = -1$ , upstream of the step location, and  $x/S = 0$ , at the step location. An agreement between the profiles at the two axial locations is an indication of the attainment of the fully developed condition. An observation of the results of Fig. 3, indicates that, indeed, the velocity profiles are coincident for the two axial locations and, therefore, can be considered fully developed for the three values of the Reynolds number shown in the figure. In fact, the fully developed condition was obtained for all the other values of the Reynolds number investigated but not shown in the figure. For the  $Re = 1000$  case, a parabolic curve was fitted through the data. The excellent quality of the fit is an indication of a laminar profile.

Figures 4a to 4c present a comparison of the measured and numerically predicted axial velocity profiles for several axial stations, for Reynolds numbers equal to 1000, 3600 and 13800. Comparisons for the other values of the Reynolds number investigated are not presented due to space limitations. In the figures, the origins of the abscissa were displaced so that a clearer picture could be obtained. The position of the axial stations is indicated on the upper part of the figure by numbers in millimeters, ranging from  $-14$  up to  $200$  mm. The origin of the axial coordinate is at the step location. Two solid lines at right angles represent the step location in the figures. Exactly below the number corresponding to each axial coordinate is a line that represents the origin for the velocity axis. The vector below the figure gives a reference in m/s for the velocity magnitude. The solid squares in the figure represent the experimentally determined velocity data, while the solid line represents the numerical predictions. The measurements reported were all conducted at the center plane of the channel, i.e., at  $z = 0$ .

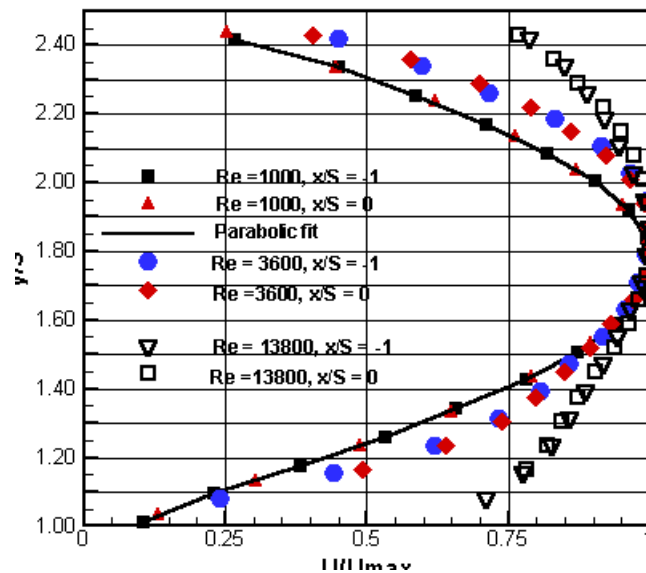


Figure 3 – Experimental, time-averaged, inlet velocity profiles for Reynolds numbers 1000, 3100 and 13800.

Figure 4a presents the results for  $Re = 1000$ . The parabolic laminar velocity profile at  $x = -14$  was used as a boundary condition for the numerical calculations. The adverse pressure gradient imposed by the sudden expansion at the step is seen to produce a large zone of recirculating flow. This zone extends almost to  $x = 200$  mm ( $x/S = 16.3$ ). The agreement between experiments and the two-dimensional calculations is excellent up to  $x = 120$  ( $x/S = 10$ ). This good agreement is a sign that three dimensional effects downstream of the step reported in Armaly et al., 1983 are not significantly disturbing the flow (at least at the center plane,  $z = 0$ , where the measurements were performed). It is worth mentioning that the comparison between measured and predicted velocity profiles presented by Armaly et al., 1983 deviate significantly for axial coordinates greater than  $x/S = 5$ , for  $Re = 1000$ . According to the authors, this was a consequence of the three dimensional character of the flow. In the present study, small deviations begin to appear only at  $x = 140$  mm ( $x/S = 11.67$ ). Also, the pocket of recirculating flow located at the top wall reported in Armaly et al., 1983, was not detected neither in our experiments nor in our numerical solutions.

Figure 4b presents results for  $Re = 3600$  what, according to Armaly et al., 1983 is at the center of the transition to turbulent flow region. The incoming velocity profile at  $x = -14$  seen in the figure, displays a shape that deviates from the laminar parabolic profile, but still does not present the more flatter profile characteristic of a turbulent flow. The region of recirculating flow is seen to be much shorter than that for the laminar case reported before, extending up to  $x = 95$  mm ( $x/S = 7.9$ ). The numerical calculations incorporating the RNG turbulence model do not predict very well the velocity profiles just downstream of the step, within the recirculation zone. The point of reattachment is calculated to be at  $x/S = 5.2$ , a value significantly different from the experimental results. Armaly et al., 1983 measured a reattachment point at  $x/S = 9.1$  for this value of the Reynolds. The discrepancy between the three results are credited to the high degree of unsteadiness of the flow at  $Re = 3600$ , as will be shown in the instantaneous results presented in Fig. 5. Beyond the point of reattachment the quality of the predictions of the turbulence model improves significantly, as can be verified in the comparisons for axial stations located at 160, 180 and 200 mm.

For flows well above the turbulence transition point, the predictions of the RNG turbulence model improve significantly. This can be seen in Fig. 4c where the results for  $Re = 13800$  are reported. It can be seen in the figure that the predictions are reasonable good even within the zone of recirculating flow. Beyond the reattachment point the

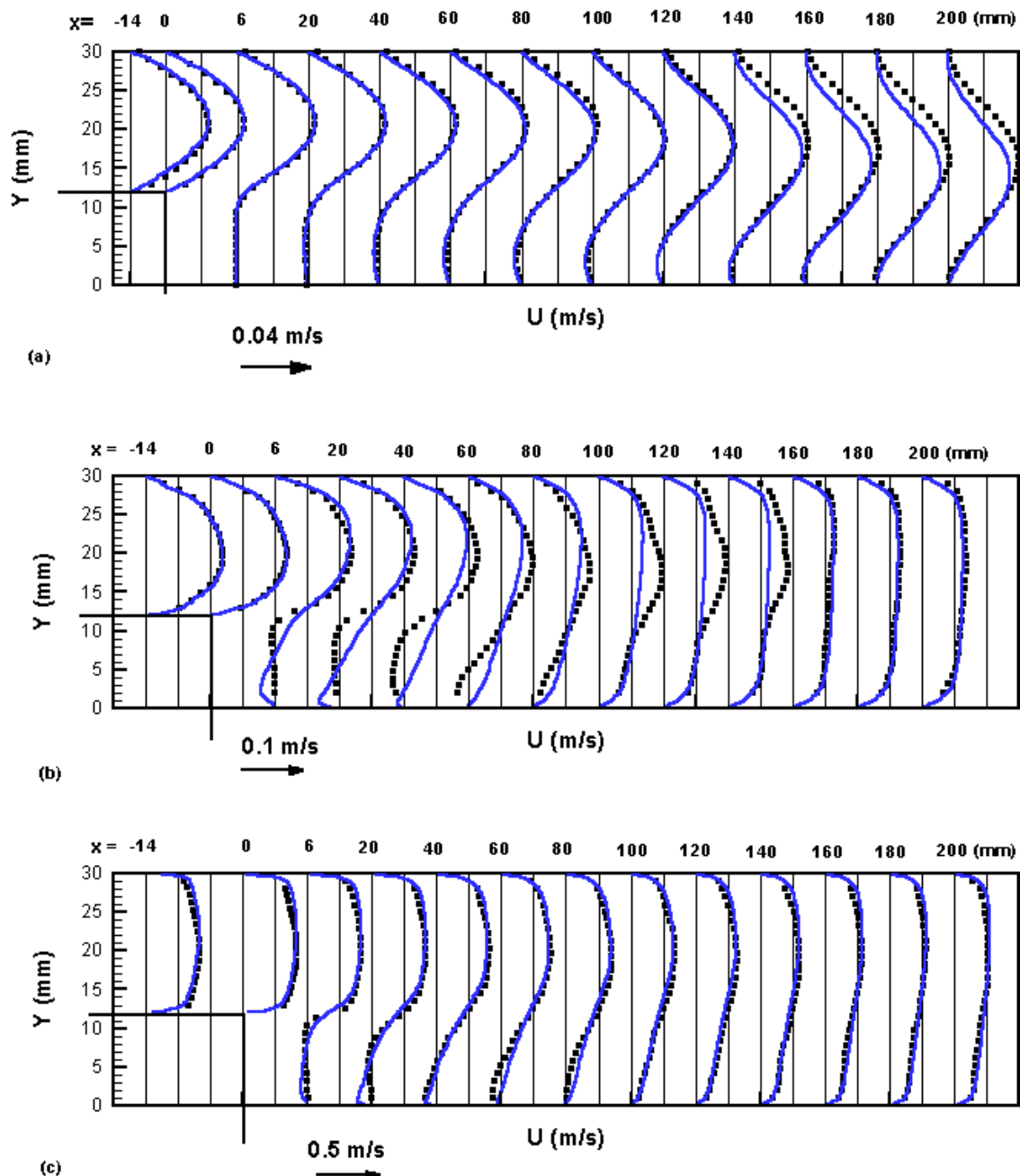


Figure 4. Numerical and experimental axial velocity profiles. (a)  $Re = 1000$ , (b)  $Re = 3600$  and (c)  $Re = 13800$ .

agreement between experiments and calculations is remarkable.

A comparison of measured and predicted reattachment points is presented in Table 1. The location of the reattachment point was determined experimentally by an inspection in all the axial velocity profiles at a cross stream coordinate  $y = 0.5$  mm, the closest point to the wall where PIV measurements were produced. In the numerical calculations the reattachment point was determined by locating the point where the wall shear stress vanished.

Table 1. Comparison between measured and predicted reattachment points

Re	$x_r/S$		
	Measured	Measured <sup>(1)</sup>	Simulation
1000	16.3	16.2	15.0
3600	7.9	9.1	5.2
6200	7.3	7.0	6.1
8800	7.8		6.5
11400	8.2		7.2
13800	8.5		7.5

(1) Armaly et al., 1983.

For comparison purposes, the results of reattachment points measured by Armaly et. al., 1983 are included in the table. The results reported in the table are in good agreement with those from Armaly et al., 1983 for the laminar and end-of- transition cases, but differ somewhat for the transition case represented by  $Re = 3600$ , as already commented. The agreement between the present experimental results and the numerical simulation are within a range of 8 to 15%, excluding the transition case. The numerical predictions of the point of reattachment are consistently lower than the measured values.

One of the main features of the PIV measurement technique is its capability of measuring instantaneous flow properties over extensive regions of the flow. Figures 5a to 5d present the instantaneous velocity vectors for a region downstream of the step starting at  $x = 50$  mm and extending up to  $x = 110$  mm. The flow Reynolds number is 3600. The colored contours represent the magnitude of the axial component of the velocity vector, and are referenced to the color legend below the figures, given in m/s. Most of the vectors measured were removed from the figure to allow a better visualization of the results. The white spots seen in the figures represent positions where no satisfactory correlations were obtained in the PIV measurements. These bad vectors were removed from the field and no attempt was made to interpolate the data to fill in these gaps. The three figures were taken with a time interval of 60 ms and belong to a series of 30 velocity fields measured and used to calculate the time-averaged results presented previously in Fig. 4. An analysis of the velocity field clearly indicates the unsteadiness of the flow. The flow close to the lower wall within the zone of recirculation is seen to completely reverse direction during the interval of the measurements. The severe unsteadiness of the flow could be responsible for the poor predicting performance of the RNG turbulence model.

## 6. Conclusions

The present study described part of an ongoing research program aimed at producing instantaneous and time averaged velocity data for validating the predictions of numerical codes incorporating turbulence models. The classical configuration formed by water flow over a backward-facing step was investigated by means of the Particle Image Velocimetry technique. Instantaneous and time-averaged velocity fields were measured for Reynolds numbers in the range from 1000 to 13800. The expansion ratio of the channel was kept fixed during the experiments at 1.67.

The comparison between experimentally and numerically determined time-averaged velocity fields was very good for the laminar regime. For the transition regime, the  $\kappa\text{-}\epsilon$  RNG turbulence model employed was not capable of predicting with reasonable accuracy the flow field within the zone of recirculating flow downstream of the backstep. Instantaneous results revealed a high degree of unsteadiness of the velocity field in this regime. The level of prediction improved considerably for the turbulent regime. The turbulence model consistently under-predicted the position of the point of reattachment of the flow.

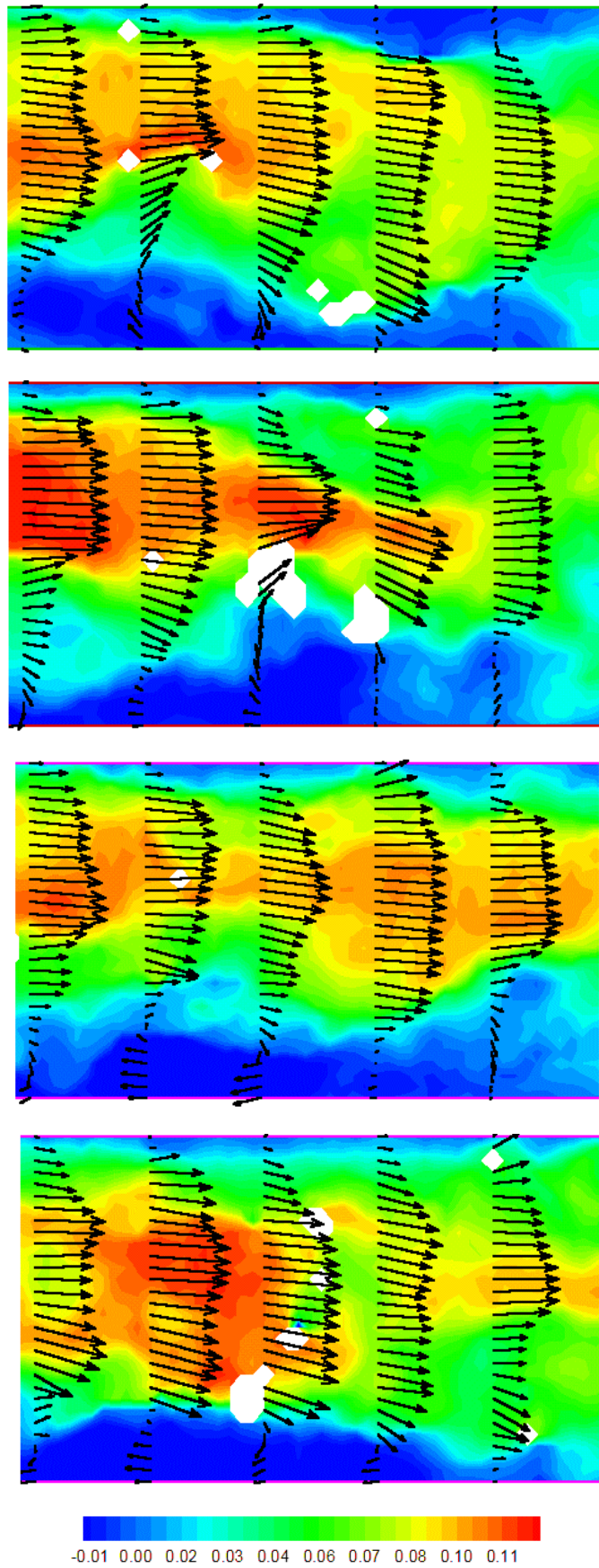


Figure5. Measured instantaneous velocity fields for  $Re= 3600$ . Axial span is  $50 \text{ mm} \leq x \leq 110 \text{ mm}$ . Time interval between figures is 60 ms.

## 7. Acknowledgments

The authors wish to acknowledge the support awarded to this research by CNPq, Brazilian Council for Research and FINEP.

## 8. References

- Armaly, B.F., Durst, F., Pereira, J.C.F., and Schönung, B., 1983, "Experimental and Theoretical Investigation of Backward-Facing Step Flow", *Journal of Fluid Mechanics*, vol. 127, pp. 473-496.
- Gomes, B.A.A., Thompsom, R.L. and Azevedo, L.F.A., 2000, "Solid Body Rotation Flow for Particle Image Velocimetry Calibration", VIII Brazilian Congress of Thermal Engineering and Science – ENCIT, Porto Alegre, Brazil CD-ROM.
- Kaiktsis, L., Karniadakis, G.E., and Orszag, A., 1996, "Unsteadiness and Convective Instabilities in Two-Dimensional Flow Over a Backward-Facing Step", *Journal of Fluid Mechanics*, vol. 321, pp. 157-187.
- Le, H., Moin, P., and Kim, J., 1997, "Direct Numerical Simulation of Turbulent Flow Over a Backward-Facing Step", *Journal of Fluid Mechanics*, vol. 330, pp. 349-347.
- Patankar, S.V., 1980, "Numerical. Heat Transfer and Fluid Flow", Hemisphere Publishing Co., New York.
- Raffel, M., Willert, C., and Kompenhans, J., 1998, "Particle Image Velocimetry – A Practical Guide", Springer-Verlag, Berlin.
- Tylli, N., Kaiktsis, and Ineichen, B., 2002, "Sidewall Effects in Flow Over a Backward-Facing Step; Experiments and Numerical Calculations", *Physics of Fluids*, vol. 14, no. 11, pp. 3835-3845.